Theoretical study of bis(N-(5-(4-methoxyphenyl)-1,3,4-oxadiazol-2-yl)ethanimidamidato)M complexes (M = Co, Ni, Cu, Zn, Pd, Cd): Structural, electronic and optical properties

Yacine Djebli, Mustafa Bencharif, Franck Rabilloud

Theoretical study of bis(N-(5-(4-methoxyphenyl)-1,3,4-oxadiazol-2-yl)ethanimidamidato)M complexes (M= Co,Ni,Cu,Zn,Pd,Cd): Structural, Electronic and Optical Properties

Yacine Djebli, Mustafa Bencharif
Laboratoire de Chimie des Matériaux, Université Constantine 1, Constantine, Algérie
m_bencharif@umc.edu.dz

Franck Rabilloud
Institut Lumière Matière, UMR5306 Université Lyon 1 – CNRS,
Université de Lyon, 69622 Villeurbanne Cedex, France
Franck.rabilloud@univ-lyon1.fr

Date: January 27th, 2016

Abstract:

We present a theoretical study of the structure and electronic and optical properties of several L_2-M compounds where L is bis(N-(5-(4-methoxyphenyl)-1,3,4-oxadiazol-2-yl)ethanimidamidato, or $C_{11}H_{11}N_4O_2$, and M = Co, Ni, Cu, Zn, Pd, Cd. Our calculations are carried out in the framework of the density-functional theory (DFT) using several families of density functionals, namely semi-local functionals, global hybrids and range-separated hybrids. Our results reproduce well the experimental data concerning the structure of the recently synthetized L_2-Cu compound. We also present the infrared spectra and absorption spectra in the visible-UV domain. The changes induced by the substitution of the Cu atom by another metal atom are investigated.

Keywords: Density Functional Theory Calculation; Time-Dependent Density Functional Theory calculation; Spectroscopic Properties; Electronic Structure

1. Introduction

Oxadiazoles constitute an important class of ligands in coordination chemistry due to their use in the synthesis of transition metal complexes. Such complexes have been demonstrated to bear important biological activities such as antibacterial [1, 2], antimycobacterial [3], antifungal [4, 5], anti-inflammatory [6, 7], analgesic [8] and anticonvulsant [9, 10]. There are three known isomers: 1,2,4-oxadiazole, 1,3,4-oxadiazole and 1,2,5-oxadiazole. However, 1,3,4-oxadiazole and 1,2,4-oxadiazole are better known, and more widely studied by researchers because of their many important chemical and biological properties [11]. Oxadiazole based ligands have been used for complexation metals, such as platinum, silver, palladium and copper [12-13]. The copper complexes with oxadiazol based ligands are important functional units in bioinorganic chemistry [14]. Copper is an essential trace element that is widely distributed in animal and plant tissues [15, 16]. It also acts as a cofactor for a number of metalloenzymes such as catalase, peroxidase, cytochrome oxidase [17, 18]. The substantial importance of copper in the biological systems has increased the interest in the coordination chemistry of copper with N, O donor ligands as biomimetic systems [19].

Recently, the compound bis(N-(5-(4-methoxyphenyl)-1,3,4-oxadiazol-2-yl)ethanimidamidato)Cu, or $(C_{11}H_{11}N_4O_2)_2$-Cu, was prepared by solvothermal synthesis using 2-amino-5-(4-methoxyphenyl)-1,3,4-oxadiazole and copper sulfate pentahydrate in an acetonitrile solution [20]. Its structure has been determined from X-ray crystallography. The Cu(II) atom lies on an inversion center and is four-coordinated in a quasi-planar structure by four N atoms of the ligands obtained from the formation of a bond between the amine N atom of the oxadiazole molecule and the nitrile C atom of the solvent (Figure 1).

In the present paper, we investigate both the electronic and optical properties of this copper complex, and also the changes in the properties when Cu is substituted by another metal. Our theoretical investigations are carried out in the framework of the density-functional theory (DFT) using several families of density functionals. Details of the calculations are given in the following section. In section 3, we present and discuss our results concerning the structural parameters of L_2-M compounds where L=$(C_{11}H_{11}N_4O_2)$ and M= Co, Ni, Cu, Zn, Pd, Cd, and the electronic and optical properties.

2. Computational Details

The geometrical optimization were performed in the framework of the density functional theory (DFT) using several density functionals, namely the second generation of type generalized gradient approximation (GGA) called BP86 [21, 22], the meta-GGA M06 [23], the global hybrids B3LYP [24, 25] and PBE0 [26], and the range-separated hybrids CAM-B3LYP [27] and ωB97x [28] which include an increasing amount of exact Hartree-Fock exchange at long range. Metal atoms were described through relativistic or quasi relativistic core potentials and the associated basis sets [29, 30], so that only the valence electrons were treated explicitly, namely the electrons of shells n=3 and 4 for Co, Ni, Cu and Zn, n=4 and 5 for Pd and Cd. The 6-31G+(d) basis sets were used for the other atoms[31].

The initial geometry was taken from the experimental data of L_2-Cu [20]. Harmonic frequency analysis was performed to guarantee that the optimized structures are local minima. Several spin multiplicities were tested for each compound, and the most stable structure was found to be a singlet or a doublet for closed and open shell systems respectively.

Further analysis and characterizations concerning electronic and optical properties were performed at B3LYP and CAM-B3LYP levels. They include calculations of both vertical and adiabatic ionization potentials, the natural population analysis (NPA) [32], and the calculation of the visible-UV absorption spectra in the framework of Time-Dependent DFT (TDDFT) [33-35]. Excited states and charge transfer character of electronic transitions were characterized by plotting the electron density difference between the excited and ground states for the main peaks.

All calculations have been performed using the Gaussian09 suite of programs [31].

3. Results and Discussion

3.1 Structure and vibrational analysis of L_2-Cu

Selected bond lengths and angles of the optimized L_2-Cu complex are shown in Table 1. They are calculated with several density functionals and compared to experiment data. All calculated values are in good agreement with the experiments, since all differences between the theoretical and experimental bond lengths are in the 0.01-0.02 Å range. For further analysis, we have selected two density functionals, namely the very popular B3LYP and its long-range corrected version CAM-B3LYP which is expected to better predict the optical properties. Bond lengths and angles implying C and N atoms are given in Table 2. The labelling of atoms can be seen in Figure 2. CAM-B3LYP is still excellent, but B3LYP is also good. Table 2 gives also the structural parameters of the free ligand, i.e. when it is not in contact to Cu. Two hydrogen atoms was added in the ligand, one H on N2 and one H on N3, to investigate the properties of the free ligand. The complexation with Cu leads to an increasing of the C-N bond lengths, except the N3-C4 bond length which is slightly shortened. The elongation is about 0.1 Angström for N1-C2 and C4-N5 bonds.

Major lines in infrared spectra are given in Table 3. The stretching vibrations of N-H, C-C, C-N are clearly identified, as well as two stretching modes implying the copper atom at 697 and 990 cm^{-1} at B3LYP level. The vibrational frequencies are slightly larger at CAM-B3LYP level, and the intensities of the major lines are stronger.

3.2 Structure and electronic properties of L_2-M, M=Co, Ni, Zn, Pd, Cd

We have substituted the copper atom by M = Co, Ni, Zn, Pd and Cd in order to study the influence of the metal and to predict the stability and properties of compounds. All complexes are found to be stable in a singlet state for M=Ni, Zn, Pd, and Cd, and in a doublet state for M=Co. After the substitution, the geometrical structure of the complex is still somewhat similar to that of L_2-Cu as shown in Figure 1. The M-N bond lengths and angles are given in Table 4. The B3LYP bonds are 0.01-0.02 Angström longer than the CAM-B3LYP values, while angles are very similar whatever the functional is used. To the best of our knowledge, no experiment data are available. The natural atomic charge and the natural electron configuration on metal atoms are given in Table 5. B3LYP and CAM-B3LYP values are similar. As expected, all metal atoms have a positive net charge, it is ranged from 0.535 to 1.239 a.u. at B3LYP level. The negative net charge on its first neighbors N atoms are larger for N3 than for N2 due to the presence of hydrogen group on N3. Interestingly, the charge on nitrogen is relatively few sensitive to the nature of the metal. The natural electron configuration of Co in the complex (Table 5) could be compared to those of the Co atom in the doublet state ($4s3d^8$), and one can conclude that the positive charge on Co is due a loss of electron in both s and d shells. The situation is similar for nickel complex when we take the doublet configuration ($4s3d^9$) as a reference. In contrast, the large positive charge on Zn and Cd is only due the loss of s-type electron, the d shell not being

perturbed. Pd losses some electrons d but gains some s and p type electrons. Let us note that in NPA analysis of transition metals, the addition of a set of p-type empty orbitals (referred to as Rydberg orbitals) to the valence orbitals mays lead in a different electronic configuration. The appropriateness of using NPA on metal transition are discussed in more details in Ref [36-38]. Here we have used the standard natural atomic orbitals as available in Gaussian09 [31].

Both the vertical (IP_v) and adiabatic (IP_a) ionization potentials are given in Table 6. The CAM-B3LYP values are systematically larger than B3LYP data. The small difference between values of IP_v and IP_a is explained by the very small deformation of the structure induced by the electron removing. The stronger deformation happens for L_2-Cu but stays small. During the ionization, the electron is extracted from the highest occupied molecular orbital (HOMO) which is a delocalized π-type orbital involving mainly C, N, and O atoms of the whole ligand. A participation of a d-type orbital on the metal occurs in the case of L_2-Pd and L_2-Ni, and to a small extend in L_2-Co and L_2-Cu. As an illustration, the HOMO of the L_2-Pd compound can be seen in Figure 3. The very similar character of the HOMO, mainly extended on the whole ligand, for all complexes leads to find IPs in a relatively narrow range of energy around 7 eV.

3.3 Absorption spectra

The absorption spectra calculated at both B3LYP and CAM-B3LYP levels for all complexes and the ligand are shown is Figure 4. The spectra have been calculated up to 8 eV, and as no transition occurs lower 3 eV, the spectra are shown in the 3-8 eV range of energy. All spectra presented in the figure give both a stick spectrum with the oscillator strength as a function of the excitation energy and a curve obtained by a Lorentzian broadening with a full width of half height of 0.05 eV.

We have calculated the spectrum of the ligand L whose the structure can be seen in Figure 2. The B3LYP spectrum can be seen at the bottom of the figure 4. It is composed of a strong transition at 4.17 eV surrounded by two weak transitions at 4.06 and 4.21 eV, and followed by several small peaks up to 6.5 eV, then several more significant peaks at 6.72 eV and in the 7-7.2 eV range of energy. Using CAM-B3LYP, the transitions in the low energy region are blueshifted by about 0.5 eV as compared to those of B3LYP, since the main transitions are calculated at 4.34, 4.59, 4.70 and 5.23 eV. In the high energy domain, a relatively strong band between 6.50 and 7.08 eV is observed.

The B3LYP spectrum of all L_2-M complexes contains many transitions well scattered on all the range of energy, and with a strong response around 4 and 7 eV. We can distinguish three different families of spectra. First, L_2-Cu, L_2-Zn and L_2-Cd present a roughly similar spectrum with two intense transitions at low energy (3.79 and 4.08 eV for L_2-Cu, 3.88 and 4.10 eV for L_2-Zn, 3.89 and 4.08 for L_2-Cd) and a strong band at about 7.1 eV. In contrast, the spectra of L_2-Ni and L_2-Pd show three peaks well separated in the low energy region (3.42, 4.08, 4.52 eV for L_2-Ni and 3.38, 4.11 and 4.63 eV for L_2-Pd), and a large band in the high energy region between 6.5 and 8 eV and composed of several peaks. Finally, the spectrum of the complex L_2-Co differs from all previous ones, as it is made of a large band in the low energy domain with mainly peaks at 3.59, 3.77, 3.90, 4.16 and 4.30 eV, and a strong transition at 7.1 eV.

When using the range-separated hybrid CAM-B3LYP which includes an increasing amount of exact Hartree-Fock exchange at long range instead of a constant and low amount as in B3LYP, the absorption spectra are modified. As expected [39], the long-range correction increases significantly

the oscillator strengths of dominant transitions, while it removes a large number of spurious states with frequently low or zero oscillator strength. Although some changes occur in the spectra, the strong responses around 4 and 7 eV still occur as a signature of the absorption by the ligand. The strong transition near 7.1 eV does not involve the metal atom and the exact position is very few sensitive to the metal. The exact position is 7.14, 7.13, 7.05, 7.13, 7.14, 7.14 for M = Co, Ni, Cu, Zn, Pd, Cd respectively, compared to the value of 7.08 eV for the free ligand. In contrast, on the low energy region the exact position of the strong transition is found to depend on the metal and located between 4 and 4.5 eV, while the transition is located at 4.70 eV in the ligand alone. The position is 4.46, 4.27, 4.43, 4.47, 4.17 and 4.44 eV for M = Co, Ni, Cu, Zn, Pd, and Cd respectively. The participation of the metal atom can be seen in Figure 5 in which the isosurface of the electron density difference between the excited and ground states for the main peaks of L_2-Pd and L_2-Cu complexes are shown. Red colored regions correspond to the depletion of the electron density during the transition while the blue regions correspond to the accumulation of electrons. The excitation at 4.17 eV in L_2-Pd involves the whole ligand and also the Pd atom as a donor. At B3LYP level, this excitation is found at 4.11 eV (see figure 5). From Figure 5, it also appears that the lowest transition at 3.38 eV obtained with B3LYP has a strong charge-transfer character since the electron is transferred from a molecular orbital involving a d-type orbital on the Pd atom and p-type orbitals from N atoms (red color zone in figure 5) to an extended zone on C and O atoms (blue color in figure 5). This type of excitations are properly described only with an asymptotically corrected functional and cannot be described with B3LYP [36]. Hence the transition seems to be a so-called spurious state due to a poor description of long-range interactions at B3LYP level. The spectra for L_2-Ni and L_2-Pd are still somewhat similar to each other. They are made of three peaks in the 4-5.5 eV range of energy (4.27, 4.91 and 5.27 eV for L-Ni, and 4.17, 4.78 and 5.28 eV for L_2-Pd). In contrast, spectra of L_2-Cu, L_2-Zn and L_2-Cd have no significant peaks in the 4.5-6 eV range of energy. L_2-Co is somewhat similar to the latter, but with a singularity as all main transitions are surrounded by several less-intense peaks at both lower and higher energies.

The influence of the long-range exchange interaction, briefly discussed above for L_2-Pd, is also significant for the other complexes. For L_2-Ni, the B3LYP transition at 3.42 eV is removed when CAM-B3LYP is used. For L_2-Cu, L_2-Zn, L_2-Cd the first transition near 3.8 eV also disappears, while the second one at about 4.1 eV is blueshifted by about 0.3 eV. In figure 5, we show the depletion and accumulation of the electron density during the transitions in the case of L_2-Cu. Using B3LYP, the transition at 3.79 V has a strong charge-transfer character since the electron is transferred from the metal and its N neighbors to a distant region on the ligand. With CAM-B3LYP, this transition does not occurs alone, since the first transition at 4.43 eV corresponds to a mixture of both B3LYP transitions at 3.79 and 4.08 eV respectively with a strong blueshift. Similarly, for L_2-Zn and L_2-Cd complexes, the CAM-B3LYP transitions at 4.43 and 4.44 eV respectively, correspond to a superposition of the two B3LYP transitions calculated at 3.88 and 4.08 eV. Finally, for L_2-Co, the absorption band between 3.5 and 4.3 eV calculated with B3LYP is substituted by a strong peak at 4.46 eV surrounded by two less-intense transitions. Interestingly, the frontier molecular orbitals calculated using B3LYP and CAM-B3LYP are somewhat similar, as shown in figure 3. However the HOMO-LUMO gap is much more significant with CAM-B3LYP. Both the increase in the gap, and the more accurate treatment of long range exchange interactions are responsible for the change in the absorption spectra. The present comparison between B3LYP and CAM-B3LYP confirmed a consensus that many functionals (including B3LYP) underestimate the charge-transfer excitation energy [40].

We have also calculated the absorption spectrum of L_2-Cu complex using others density functionals, namely BP86, PBE0 and ωB97x. The spectrum obtained at PBE0 was found to be somewhat similar to that calculated at B3LYP level, while the BP86's spectrum exhibits a redshift of about 0.4 eV

of the main transitions, and the occurrence of a strong transition at 4.5 eV. The spectrum obtained using ωB97x is very similar to that of CAM-B3LYP except a blueshift of 0.2 eV of the whole spectrum.

4. Conclusion

We have presented a theoretical study based on DFT and TDDFT calculations on metal (M=Co, Ni, Cu, Zn, Pd, Cd) complex with bis(N-(5-(4-methoxyphenyl)-1,3,4-oxadiazol-2-yl)ethanimidamidato). The structural parameters for L_2-Cu complex are in excellent agreement with the experimental data, while no experimental values are available for the other complexes. The UV-visible absorption spectra, calculated with both a global hybrid functional and a long-range corrected hybrid functional, exhibit a strong response around 4 and 7 eV for all complexes. However, a more careful analysis of the spectra leads to distinguish three families of complexes. The first one is composed by L_2-Cu, L_2-Zn and L_2-Cd, for which the spectrum exhibits an unique transition at low energy, the second family consists of L_2-Ni and L_2-Pd, characterized by three transitions below 5.5 eV, and the last family only contains L_2-Co with a somewhat singular spectrum due to the presence of many less-intense peaks at both lower and higher energies.

References

[1] B.S. Holla, R. Gonsalves, S .Shenoy, Synthesis and antibacterial studies of a new series of 1,2-bis(1,3,4-oxadiazol-2-yl)ethanes and 1,2-bis(4-amino-1,2,4-triazol-3-yl)ethanes, Eur. J. Med. Chem. 35 (2000) 267–271.

[2] G. Sahin, E. Palaska, M. MelikeEkizoglu, M. Ozalp, Synthesis and antimicrobial activity of some 1,3,4-oxadiazole derivatives, II Farmaco 57 (2002) 539–545.

[3] F. Macaev, G. Rusu, S. Pogrebnoi, A. Gudima, E. Stingaci, L. Vlad , N. Shvets, F. Kandemirli, A. Dimoglo, R.Reynolds, Synthesis of novel 5-aryl-2-thio-1,3,4-oxadiazoles and the study of their structure-anti-mycobacterial activities, Bioorg Med Chem 13 (2005) 4842–4850.

[4] Tale, R.H., Rodge, A.H., Keche, A.P., Hatnapure, G.D., Padole, P.R., Gaikwad, G.S. and Turkar, S.S. Synthesis and Anti-Bacterial, Anti-Fungal Activity of Novel 1,2,4-Oxadiazole, Journal of Chemical and Pharmaceutical Research, 3 (2011) 496-505.

[5] X.J. Zou, L.H. Lai, G.Y. Jin, Z.X. Zhang , Synthesis, fungicidal activity, and 3D-QSAR of pyridazinone-substituted 1,3,4-oxadiazoles and 1,3,4-thiadiazoles, J Agri. Food Chem. 50 (2002) 3757–3760.

[6] M.M Burbuliene, V. Jakubkiene, G. Mekuskiene, E. Udrenaite, R. Smicius, P. Vainilavicius, Synthesis and anti-inflammatory activity of derivatives of 5-[(2-disubstitutedamino-6-methyl-pyrimidin-4-yl)-sulfanylmethyl]-3H-1,3,4-oxadiazole-2-thiones, II Farmaco 59 (2004) 747–767.

[7] E. Palaska, G. Sahin, P. Kelicen, N.T. Durlu, G. Altinok, Synthesis and anti-inflammatory activity of 1-acylthiosemicarbazides, 1,3,4-oxadiazoles, 1,3,4-thiadiazoles and 1,2,4-triazole-3-thiones, Farmaco 57 (2002) 101–107.

[8] M. Amir, K. Shikha , Synthesis and anti-inflammatory, analgesic, ulcerogenic and lipid peroxidation activities of some new 2-[(2,6-dichloroanilino) phenyl]acetic acid derivatives, Eur. J. Med. Chem. 39 (2004) 535–545.

[9] A. Zarghi, A. Sayyed, M. Tabatabai, A. Faizi, P. Ahadian, V. Navabi , A. Zanganeh , A. Shafiee, Synthesis and anticonvulsant activity of new 2-substituted-5-(2-benzyloxyphenyl)-1,3,4-oxadiazoles, Bioorg. Med. Chem. Lett. 15 (2005) 1863–1865.

[10] A. Almasirad, A. Sayyed, M. Tabatabai, A. Faizi, N. Kebriaeezadeh, A. Mehrabi, A. Dalvandie, A. Shafiee, Synthesis and anticonvulsant activity of new 2-substituted-5- [2-(2-fluorophenoxy)phenyl]-1,3,4-oxadiazoles and 1,2,4-triazoles, Bioorg. Med. Chem. Lett. 14 (2004) 6057–6059.

[11] D. S. Musmade, S.R. Pattan, M. S. Yalgatti, Oxadiazole a nucleus wih versatile biological behavior, Int. J. Pharmaceutical Chemistry 5 (2015) 11-20.

[12] C. Richardson, P.J. Steel, The first metal complexes of 3,3'-bi-1,2,4-oxadiazole: A curiously ignored ligand, Inorg. Chem. Commun 10 (2007) 884.

[13] M. Singh, V. Aggarwal, U.P. Singh, N.K. Singh, Synthesis, spectroscopic and crystal structure investigation of $[Cu(bzsmp)_2Cl_2]$;{bzsmp = 2-benzylsulfanyl-5-(2-methoxyphenyl)-1,3,4-oxadiazole}: cyclization of N^2-[bis(benzylsulfanyl)methylene]-2-methoxybenzohydrazide to 2-benzylsulfanyl-5-(2-methoxyphenyl)-1,3,4 -oxadiazole during complexation, Polyhedron 28 (2009) 195.

[14] A. Terenzi, G. Barone, A.P. Piccionello, G. Giorgi, A. Guarcello, P. Portanova, G. Calvaruso, S. Buscemi, N. Vivona*b* and A. Pace, Synthesis, characterization, cellular uptake and interaction with native DNA of a bis(pyridyl)-1,2,4-oxadiazole copper(II) complex, Dalton Trans. 39 (2010) 9140–9145.

[15] E. Gaggelli, H. Kozlowski, D. Valensin, G. Valensin, Copper homeostasis and neurodegenerative disorders (Alzheimer's, prion, and Parkinson's diseases and amyotrophic lateral sclerosis), Chem. Rev. 106 (2006) 1995.

[16] E.L. Que, D.W. Domaile, C.J. Chang, Metals in Neurobiology Probing Their Chemistry and Biology with Molecular Imaging, Chem. Rev. 108 (2008) 1517-1549.

[17] N. Ito, S.E. Phillips, C, Stevens, Z.B. Ogel, M.J. Mcpherson, J.N. Keen, K.D. Yadav, P.F. Knowles, Novel thioether bond revealed by a 1.7 A crystal structure of galactose oxidase, Nature 350 (1991) 87-90.

[18] J.W. Whittaker, Free Radical Catalysis by Galactose Oxidase, Chem. Rev. 103 (2003) 2347-2364.

[19] M. Senjuti, N. Barnali, M. Ritwik, S Yeasin, Ch. Sudipta, B. Sujan, M.K. Tapan, M. Debadrita, G. Sanchita, Syntheses, crystal structures, spectral study and DFT calculation of three new copper(II) complexes derived from pyridoxal hydrochloride, N,N-dimethylethylenediamine and N,N-diethylethylenediamine, J. Molecular Structure 1088 (2015) 38–49 .

[20] Y. Djebli, S. Mosbah, S. Boufas, L. Bencharif, T. Roisnel, bis {N-[5-(4-methoxyphenyl)-1,3,4-oxadiazole-2-yl]ethanimidamidato}copper(II), Acta Crystallographica E66 m410 (2010).

[21] A. D. Becke, Density-functional exchange-energy approximation with correct asymptotic-behavior, Phys. Rev. A 38 (1988) 3098-3100.

[22] J. P. Perdew, Density-functional approximation for the correlation energy of the inhomogeneous electron gas, Phys. Rev. B 33 (1986) 8822-8824.

[23] Y. Zhao and D. G. Truhlar, The M06 suite of density functionals for main group thermochemistry, thermochemical kinetics, noncovalent interactions, excited states, and transition elements: two new

functionals and systematic testing of four M06-class functionals and 12 other functionals, Theor. Chem. Acc. 120 (2008) 215-41.

[24] A. D. Becke, Density-functional thermochemistry. III. The role of exact exchange, J. Chem. Phys. 98 (1993) 5648-5652.

[25] C. Lee, W. Yang, and R. G. Parr, Development of the Colle-Salvetti correlation-energy formula into a functional of the electron density, Phys. Rev. B 37 (1988) 785-789.

[26] C. Adamo and V. Barone, Toward reliable density functional methods without adjustable parameters: The PBE0 model, J. Chem. Phys. 110 (1999) 6158-6169.

[27] T. Yanai, D. Tew, and N. Handy, A new hybrid exchange-correlation functional using the Coulomb-attenuating method (CAM-B3LYP), Chem. Phys. Lett. 393 (2004) 51-57.

[28] J.-D. Chai and M. Head-Gordon, Systematic optimization of long-range corrected hybrid density functionals, J. Chem. Phys. 128 (2008) 084106.

[29] M. Dolg, U. Wedig, H. Stoll, H. Preuss, J. Chem. Phys. 86 (1987) 866.

[30] D. Andrae, U. Haeussermann, M. Dolg, H. Stoll, H. Preuss, Theor. Chim. Acta 77 (1990) 123.

[31] Gaussian09, Revision D.01, M.J. Frisch et al., Gaussian, Inc., Wallingford CT, 2013.

[32] A. E. Reed, F. Weinhold, J. Chem. Phys. 78 (1983) 4066.

[33] E. Runge, E.K.U. Gross, Density-Functional Theory for Time-Dependent Systems. Phys. Rev. Lett. 52 (1984) 997−1000.

[34] M.E. Casida, Time-Dependent Density-Functional Response Theory For Molecules, in: Recent Advances in Density Functional Methods. Part I; Chong, D. P., Ed.; World Scientific: Singapore, 1995; p 155.

[35] R. van Leeuwen, Key Concepts in Time-Dependent Density-Functional Theory, Int. J. Mod. Phys. B 15 (2001) 1969−2023.

[36] C. R. Landis, F. Weinhold, Valence and Extra-Valence Orbitals in Main Group and Transition Metal Bonding, J. Comput. Chem. 28 (2007) 198-203.

[37] C. R. Landis, R. P. Hughes, F. Weinhold, Bonding Analysis of TM(cAAC)$_2$ (TM = Cu,Ag, and Au) and the importance of reference State, Organometallics 34 (2015) 3442-3449.

[38] B. K. Chethana, D. Lee, S. H. Mushri, First Principle Investigation into the Metal Catalysed 1,2 Carbon Shift Reaction for the Epimerization of Sugars, J. Mol. Catalysis A : Chemical 410 (2015) 66-73.

[39] F. Rabilloud, Assessment of the Performance of Long-Range-Corrected Density Functionals for Calculating the Absorption Spectra of Silver Clusters, J. Phys. Chem. A 117 (2013) 4267-4278.

[40] A. Dreuw, M. Head-Gordon, Single-reference ab initio methods for the calculation of excited states of large molecules, Chem. Rev. 105 (2005) 4009-4037.

Table 1. Selected bond lengths (in Angström) and angles (in degrees) of L_2-Cu calculated with several functionals and compared to experiment data [20].

	B3LYP	CAM-B3LYP	BP86	M06	PBE0	wB97X	EXP.
Cu1-N2(Å)	1.959	1.942	1.951	1.939	1.943	1.947	1.940
Cu1-N3(Å)	1.960	1.945	1.955	1.944	1.945	1.952	1.945
N2-Cu1-N3(°)	91.58	91.47	91.05	91.2	91.4	91.65	92.61
N3-Cu1-N2'(°)	88.42	88.53	88.95	88.8	88.6	88.35	87.39
N2-Cu1-N3-N2'(°)	180.	180.	180.	180.	180.	180.	180.

Table 2. Selected bond lengths (in Angström) and angles (in degrees) of free L=($C_{11}H_{11}N_4O_2$) calculated at B3LYP and CAM-B3LYP levels. Bond and angle values in L_2-Cu complex are also given in parenthesis for comparison to experimental data [20].

	B3LYP	CAM-B3LYP	Expt
bonds (A°)			
N1-C2	1.431 (1.317)	1.428 (1.311)	1.311
C2-N3	1.352 (1.350)	1.350 (1.344)	1.346
N3-C4	1.290 (1.321)	1.283 (1.317)	1.329
C4-N5	1.390 (1.334)	1.383 (1.325)	1.325
Angle (°)			
N1-C2-C4	120.7 (125.44)	120.55 (125.46)	125.49
C2-N3-C4	126.0 (119.07)	125.37 (118.85)	118.12
N3-C4-N5	134.5 (133.44)	134.0 (133.31)	133.28
N1-C2-N3-C4	170.8 (180.0)	170.8 (180.0)	177.4
C2-N3-C4-N5	174.6	175.4	177.4

Table 3. Selected vibrational frequencies and Infrared intensities of L_2-Cu complex calculated using B3LYP and CAM-B3LYP.

Vibrational assignment	B3LYP		CAM-B3LYP	
	Frequency (cm^{-1})	IR intensity (10^3 m mol^{-1})	Frequency (cm^{-1})	IR intensity (10^3 m mol^{-1})
ν(N-H) (stretching)	3500	254	3540	295
ν(H2C-H) (stretching)	3039	124	3068	99
ν(C=C) (stretching)	1674	216	1689	520
ν(C-N) (stretching)	1638	626	1647	804
ν(C-N) (stretching)	1579	773	1614	1281
ν(C-CH3) (stretching)	1486	227	1523	231
ν(Cu-N<) (stretching)	990	139	1029	247
ν(=C-H) (bending)	877	148	900	175
ν(Cu-NH) (stretching)	697	29	713	27

Table 4. Selected bond lengths (in Angström) and angles (in degrees) of L_2-M (M = Co, Ni, Zn, Pd, Cd) calculated at B3LYP and CAM-B3LYP levels.

	B3LYP	CAM-B3LYP
Co1-N2	1.886	1.878
Co1-N3	1.894	1.886
N2-Co1-N3	90.85	90.86
N3-Co1-N4	89.15	89.14
N2-Co1-N3-N4	180.	180.
Ni1-N2	1.869	1.857
Ni1-N3	1.878	1.868
N2-Ni1-N3	90.29	90.28
N3-Ni1-N2’	89.71	89.72
N2-Ni1-N3-N2’	180.	180.
Zn1-N2	2.052	2.028
Zn 1-N3	2.002	1.992
N2- Zn 1-N3	92.83	92.71
N3- Zn 1-N2’	87.17	87.29
N2- Zn -N3-N2’	180.	180.
Pd1-N2	2.001	1.989
Pd 1-N3	2.021	2.008
N2- Pd -N3	91.86	91.83
N3- Pd –N2’	88.14	88.17
N2- Pd 1-N3-N2’	180.	180.
Cd1-N2	2.255	2.230
Cd1-N3	2.202	2.187
N2-Cd1-N3	97.18	97.1
N3-Cd1-N4	82.82	82.9
N2-Cd1-N3-N4	180.	180.

Table 5. Atomic charges (a.u.) and electron configuration in L_2-M (M=Co,Ni,Cu,Zn,Pd,Cd) complexes using the natural population analysis (NPA).

	Atomic charge		Electron configuration	
	B3LYP	CAM-B3LYP	B3LYP	CAM-B3LYP
Co	0.630	0.609	$4s^{0.36}3d^{7.65}4p^{0.40}4d^{0.02}5p^{0.01}$	$4s^{0.36}3d^{7.57}4p^{0.39}4d^{0.02}5p^{0.01}$
N2	-0.405	-0.394		
N3	-0.683	-0.756		
Ni	0.578	0.585	$4s^{0.36}3d^{8.63}4p^{0.14}4d^{0.01}5p^{0.28}5d^{0.01}$	$4s^{0.36}3d^{8.62}4p^{0.01}4d^{0.01}5p^{0.42}5d^{0.01}$
N2	-0.392	-0.403		
N3	-0.714	-0.728		
Cu	0.897	0.908	$4s^{0.39}3d^{9.30}4p^{0.43}4d^{0.01}5p^{0.01}$	$4s^{0.37}3d^{9.27}4p^{0.42}4d^{0.01}5p^{0.01}$
N2	-0.598	-0.475		
N3	-0.797	-0.811		
Zn	1.211	1.217	$4s^{0.42}3d^{9.96}4p^{0.40}4d^{0.01}$	$4s^{0.40}3d^{9.96}4p^{0.41}4d^{0.01}$
N2	-0.525	-0.536		
N3	-0.883	-0.893		
Pd	0.535	0.548	$5s^{0.40}4d^{8.77}5p^{0.26}6s^{0.01}5d^{0.01}6p^{0.01}$	$5s^{0.40}4d^{8.75}5p^{0.27}6s^{0.01}5d^{0.01}6p^{0.10}$
N2	-0.385	-0.397		
N3	-0.708	-0.723		
Cd	1.239	1.253	$5s^{0.45}4d^{9.96}5p^{0.35}5d^{0.01}$	$5s^{0.42}4d^{9.95}5p^{0.36}5d^{0.01}$
N2	-0.515	-0.625		
N3	-0.881	-0.895		

Table 6. Vertical and adiabatic ionization potentials (in eV).

$IP_{v(a)}$	L2-Co	L2-Ni	L2-Cu	L2-Zn	L2-Pd	L2-Cd
B3LYP	6.993 (6.857)	6.450 (6.422)	7.325 (6.855)	6.694 (6.585)	6.421 (6.34)	6.639 (6.542)
CAM-B3LYP	7.537 (7.374)	6.884 (6.778)	7.673 (7.047)	7.256 (7.129)	6.887 (6.791)	7.238 (7.102)

Figure 1. Structure of the complex bis {N-[5-(methoxyphenyl)-1,3,4-oxadiazole-2-yl]ethanimidamidato}Cu(II) $(C_{11}H_{11}N_40_2)_2Cu$.

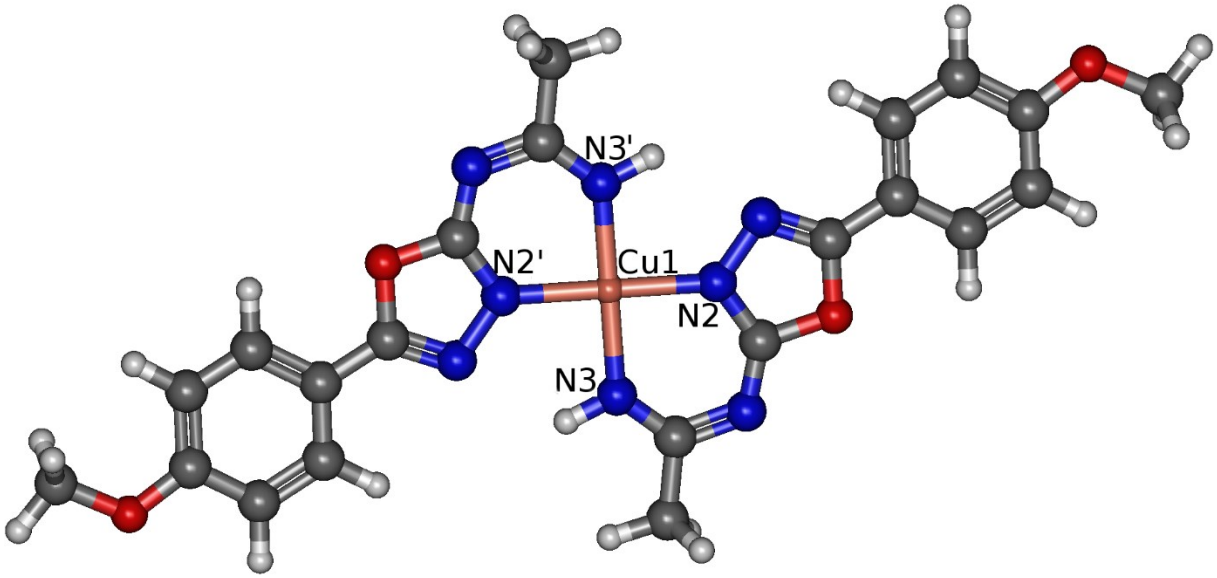

Figure 2. Structure of the ligand L=$(C_{11}H_{11}N_40_2)$, N-[5-(methoxyphenyl)-1,3,4-oxadiazole-2-yl]ethanimidamidato**.**

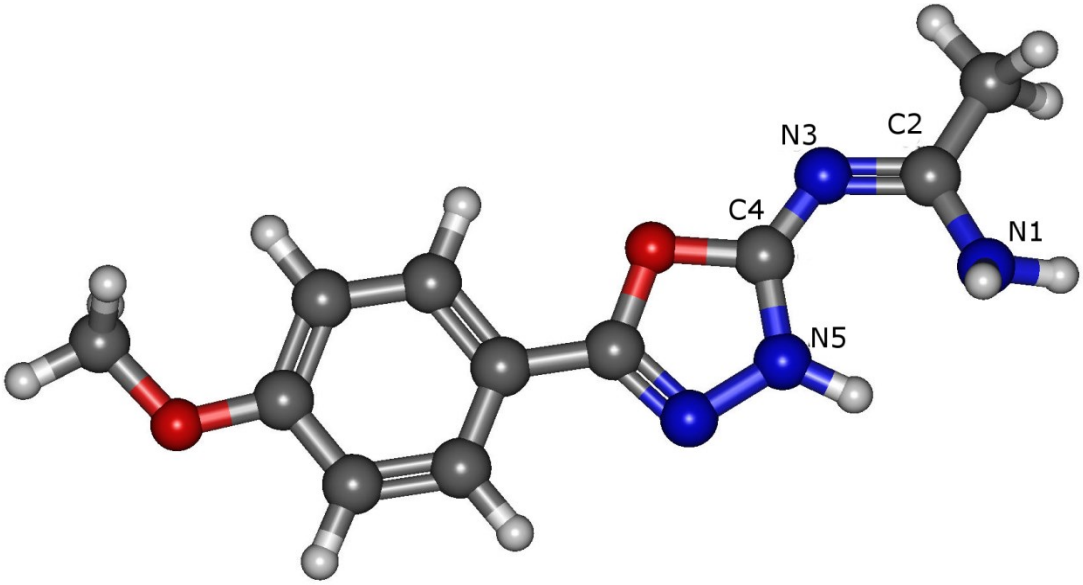

Figure 3. Energy levels and shapes of the relevant frontier orbitals of L_2-Pd.

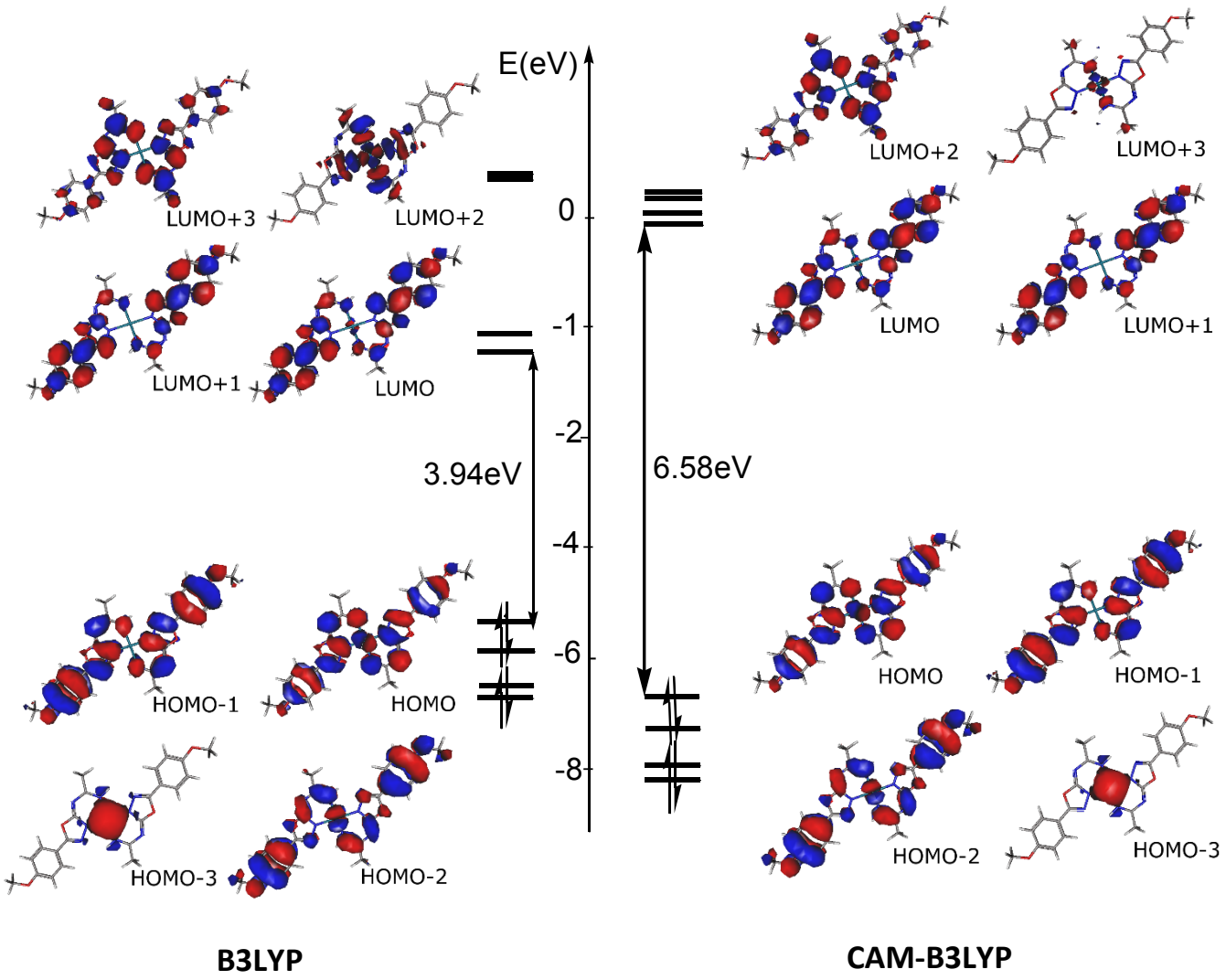

Figure 4. Calculated absorption spectra of the ligand L=($C_{11}H_{11}N_4O_2$) and L_2-M (M=Co, Ni, Cu, Zn, Pd, Cd) complexes using B3LYP and CAM-B3LYP functionals.

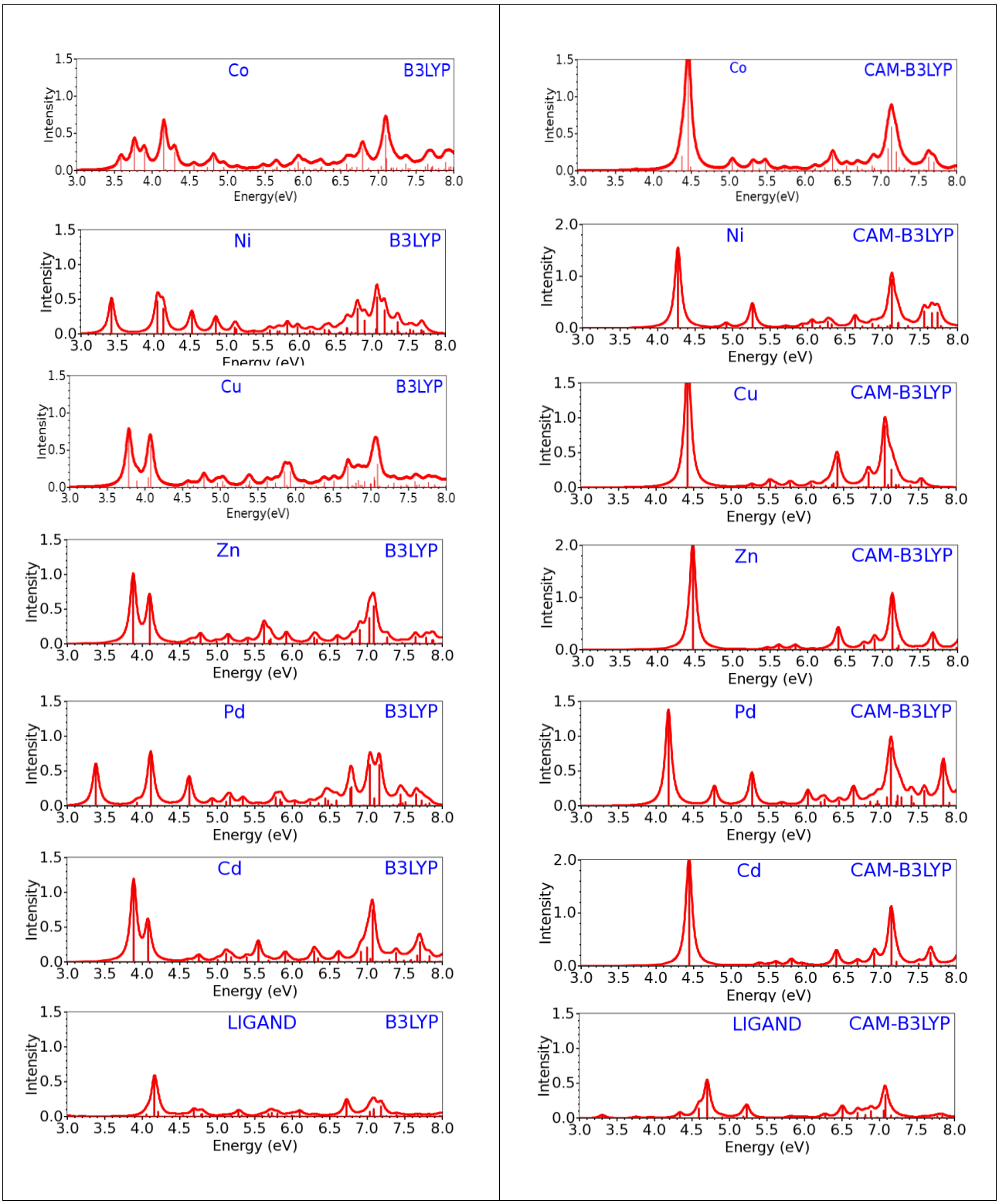

Figure 5. Isosurface of the electron density difference between the excited and ground states for some of the main peaks of L_2-Pd and L_2-Cu complexes. Red colored regions correspond to the depletion of the electron density during the transition while the blue regions correspond to the accumulation of electrons (isovalue = 0.0003 a.u.).